Biophysical Reports

ARTICLE

Modeling multiple duplex DNA attachments in a force-extension experiment

Allan Raudsepp,[1] Martin A. K. Williams,[1,2,*] and Geoffrey B. Jameson[1,2]
[1]School of Fundamental Sciences, Massey University, Palmerston North, New Zealand and [2]MacDiarmid Institute, Victoria University of Wellington, Wellington, New Zealand

ABSTRACT Optical tweezers-based DNA stretching often relies on tethering a single end-activated DNA molecule between optically manipulated end-binding beads. Measurement success can depend on DNA concentration. At lower DNA concentrations tethering is less common, and many trials may be required to observe a single-molecule stretch. At higher DNA concentrations tethering is more common; however, the resulting force-extensions observed are more complex and may vary from measurement to measurement. Typically these more complex results are attributed to the formation of multiple tethers between the beads; however, to date there does not appear to have been a critical examination of this hypothesis or the potential usefulness of such data. Here we examine stretches at a higher DNA concentration and use analysis and simulation to show how the more complex force-extensions observed can be understood in terms of multiple DNA attachments.

SIGNIFICANCE Optical tweezers-based DNA stretching often relies on tethering a single end-activated DNA molecule between optically manipulated end-binding beads. Resulting measurements can show some complexity and may vary from run to run. These more complex, variable results are typically attributed to the formation of multiple DNA tethers between the beads. In this work this assumption is critically examined, and it is demonstrated, using a combination of simulation and experiment, that this untested attribution is not unreasonable.

INTRODUCTION

DNA is a biopolymer of fundamental biological importance. While research has traditionally focused on this biopolymer's biology and chemistry, more recent research has begun to examine the molecule's physics (1). DNA is somewhat unique among polymers in that it can be synthesized with a known monomer sequence with activated "handles" at the ends. Most biophysical studies (including our own) focus on double-stranded DNA (dsDNA) in which each polymer of the double-stranded duplex has one handle. These handles can selectively bind, either chemically or physically, to treated substrates and this selectivity can be used to isolate individual chains, allowing researchers to study the physics of single molecules. A popular single-molecule experiment is a stretch (1–6). In addition to enabling more sophisticated experiments with clear biological relevance (7–15), the so-called overstretch transition of dsDNA yields a molecular standard for force calibration (16,17). In the most common variation of this experiment, the DNA is bound to two surfaces via the handles, the surfaces are separated, and force on the surfaces with surface separation, or equivalently molecule extension, is inferred. While this experiment is simple, the interpretation is not without ambiguity. Binding between the handles and surfaces relies on making contact between the two and depends on the random thermal diffusion of the polymer. If sufficient DNA is present, multiple DNA duplexes can attach and bridge the gap between the surfaces, and this could be expected to perturb the force-extension measurement, which introduces uncertainty. The effects of these multiple attachments on force-extension measurements in a typical dual optical trap experiment are investigated here.

The wormlike chain (WLC) model describes the extensibility of semiflexible linear polymers (2–4,18,19). This model depends on the polymer contour length, l_c, and the persistence length, l_p, and relates the extension force, F, to the extension, d':

Submitted October 25, 2021, revisions received December 20, 2021; accepted for publication January 28, 2022.

*Correspondence: m.williams@massey.ac.nz

Editor: Jörg Enderlein.

https://doi.org/10.1016/j.bpr.2022.100045

$$F = \frac{k_B T}{l_p}\left(\frac{1}{4}\left[\left(1-\frac{d'}{l_c}\right)^{-2}\right]+\frac{d'}{l_c}-\frac{1}{4}\right). \quad (1)$$

This force-extension relation can be probed using optical tweezers, magnetic tweezers, or atomic force spectroscopy. In a typical dual optical trap experiment, the chain is attached to the ends of two optically trapped beads (20–23). These beads are progressively separated, and d' and F are inferred from the location of the beads. This is shown schematically in Fig. 1 *A*. Here, the chain is represented schematically by a spring which is stretched between a bigger bead with radius r_1 and a smaller bead with radius r_2. Because standard gradient traps, commonly used in stretching experiments, do not impart torque to the beads, the beads will orient to minimize torque, which occurs when the spring is aligned with the bead centers. In this configuration, the spring extension d' is equal to the surface-to-surface separation of the beads d. Fig. 1 *B* shows the force-extension expected. Fig. 1 *C* shows beads connected by a pair of identical springs. Again, the beads will orient to minimize torque, which (for this fairly contrived example) occurs when the springs are parallel. Here, for a given d the chain is stretched by an excess extension $\Delta d = \Delta d_1 + \Delta d_2$, so total extension is $d' = d + \Delta d$ and force-extension is

$$F = N\frac{k_B T}{l_p}\left(\frac{1}{4}\left[\left(1-\frac{d+\Delta d}{l_c}\right)^{-2}\right]+\frac{d+\Delta d}{l_c}-\frac{1}{4}\right), \quad (2)$$

where $N = 2$ for a two-spring configuration. Fig. 1 *B* shows the force-extension predicted. Notably, if $N = 2$ and $d + \Delta d \approx d$, which can occur if the chain is much longer than the bead diameter, or if the attachment sites are closely spaced, then $F(N = 2, l_p) \approx F(N = 1, l_p/2)$; that is, the effective persistence length of this two-chain system is half that of a single-chain system (24). In general, the springs will not be parallel at equilibrium and the interpretation of an excess extension Δd is less obvious. In this case Eq. 2 will be, at best, an approximation. Multiple attachments have been directly investigated using magnetic tweezers-based stretching (24–26). In these experiments the effects of twisting or braiding of two chains tethered between a bead and a planar surface on the resulting force-extension measurements were examined. Only cases where the chains can be assumed to be approximately parallel (like that shown Fig. 1 *C*) appear to be examined in detail here. In general, attachment sites can be expected to be distributed over the surface of the beads and more than two chains may be present. The presence of an unknown number of attachments can be expected to complicate interpretation, and this problem has been examined in single-molecule force spectroscopy bond strength studies with the view to mitigating its effects (27). In the current work we consider multiple chains attached at a biased distribution of sites between optically trapped beads and demonstrate that the multichain WLC approximation given by Eq. 2 can be used to parameterize both simulated and experimental force-extension data for reference DNA. We expect that these observations will help us to better understand these often undesired and underreported measurements.

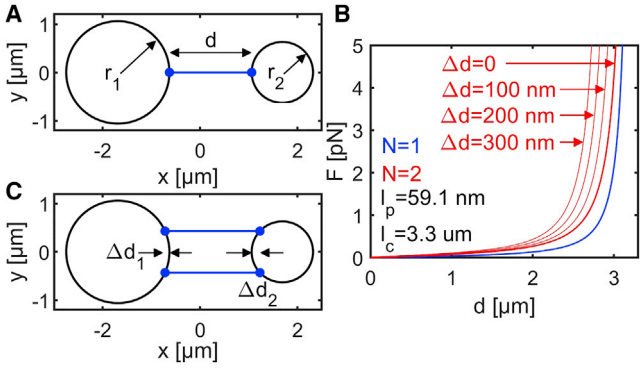

FIGURE 1 (*A* and *C*) Model setup for a dual-trap multiple duplex DNA attachment simulation. (*B*) Calculated force-extensions for one ($N = 1$) and two ($N = 2$) attachments at the torque minimum. The two-attachment force-extension depends on attachment location, which is parameterized by the excess extension Δd.

MATERIALS AND METHODS

DNA stretching and imaging experiments were carried out on an inverted microscope (Eclipse TE2000-U; Nikon, Tokyo, Japan) equipped with holographic optical tweezers (Arryx, Chicago, IL, USA). The setup includes a fixed 5 W $\lambda = 1032$ nm infrared laser, a spatial light modulator (phase-only; Boulder Nonlinear Systems, Boulder, CO, USA) steered 2 W $\lambda = 1064$ nm infrared laser, and a high-speed camera (Neo; Andor, Belfast, UK). A high numerical aperture (NA) water immersion objective (plan apo, magnification $60\times$; NA = 1.2; Nikon) was used for focusing and trapping. The dsDNA stretched here was studied previously in (21,22). One strand of the 10 kbp dsDNA used contains 2244 adenine, 2019 thymine, 3271 guanine, and 2517 cytosine bases, for a total of 10,051 bases, with the other strand being its reverse complement. Each strand of the double-stranded duplex is terminated by either biotin or digoxigenin handles which bind to streptavidin and anti-digoxigenin, respectively, by physisorption. Following the protocol used in (21,22), DNA was incubated in TSB (50 mM Tris, 150 mM NaCl, 1 mM EDTA, pH 7.6) with $2r_S = 1.26$ μm streptavidin-coated beads (Spherotec, Green Oaks, IL, USA) for at least 1 h and combined with $2r_B = 2.12$ μm anti-digoxigenin-coated beads (Spherotec) in TSB in a well slide.

Typical images of the beads during a DNA stretching experiment are shown in Fig. 2 *A*. The bigger (*B*) digoxigenin bead is on the left in the fixed $\lambda = 1032$ nm trap and the smaller (*S*) streptavidin bead is on the right in the steered $\lambda = 1064$ nm trap. This steered trap is displaced through a triangular wave, periodically bringing the beads very close. When the beads are close, DNA bound to the smaller streptavidin bead via the biotin handle may bind to the bigger anti-digoxigenin bead via the digoxigenin handle. If this occurs the bigger bead will be displaced toward the smaller bead when the beads are remote, as

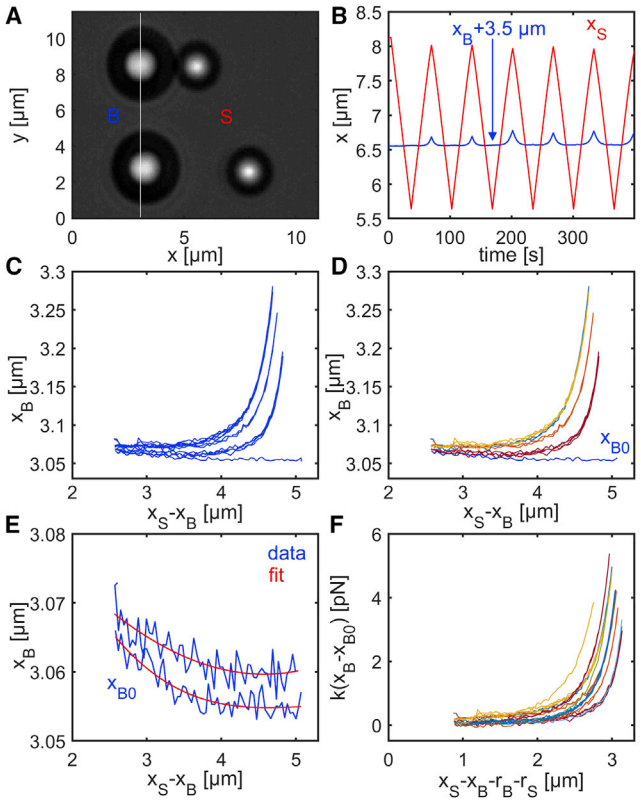

FIGURE 2 (*A*) Pair of images showing the big (B) and small (S) beads during a DNA stretch experiment. (*B*) Tracked *x*-positions of the big and small beads during repeated stretches. (*C*) Displacement separation for the data in (*B*). (*D*) Displacement separation for the data in (*C*) colored according to continuity. (*E*) Background displacement-separation measurements when no DNA is present with a polynomial fit. (*F*) Force extension for the data in (*D*) with background correction shown in (*E*); a second set of force-extensions for the same bead pair is included.

can be seen occurring in Fig. 2 *A*. The positions of both beads are determined using center-of-mass tracking. The beads' *x*-displacement is shown in Fig. 2 *B* and these data are replotted in Fig. 2 *C*, which shows the displacement of the bigger bead x_B with the beads' center-to-center separation $x_S - x_B$. Here, we observed four different trajectories during the repeated approaches. These separate trajectories are identified using continuity arguments and are more clearly distinguished in Fig. 2 *D*. The data identified as x_{B0} was measured during the beads' initial approach ($t = 0 - 25$ s) when no DNA is attached. Naïvely, it might be assumed that because the beads are not attached, the bigger bead will not move as the smaller bead approaches. Some movement is observed. This movement is probably due to 1) an interaction between the big bead and steered trap and 2) tracking errors associated with overlap between the images of the beads. This "background" measurement is important as it informs on the behavior when no DNA is present. The measurements shown in Fig. 2 *B* were repeated with the same pair of beads. The second background is plotted along with the background shown in Fig. 2 *D* along with polynomial fits in Fig. 2 *E*. It is notable that the backgrounds are offset slightly, suggesting that some drift is present. Force *F* with bead surface-to-surface separation *d* was calculated according to

$$d = x_S - x_B - r_B - r_S, \tag{3}$$

$$F = k(x_B - x_{B0}(d)), \tag{4}$$

where *k* is the optical trap stiffness of the fixed trap, which is assumed to be $k = 22$ pN/μm for all measurements here and $x_{B0}(d)$ is approximated by a polynomial; Fig. 6 *F* shows resulting force-extensions (or, more accurately, force separation).

In practice, the radii of the beads r_B and r_S will be uncertain by Δr and, due to drift after background acquisition, forces will be uncertain by ΔF. Determining Δr and ΔF independently, with the accuracy required to test the model, is experimentally difficult. Instead these parameters will be determined from the single duplex stretches themselves: 190 stretches for 42 bead pairs are reported here.

RESULTS

Simulation

We consider two beads with centers at $\mathbf{D}_1 = -D_1\hat{\mathbf{x}}$ and $\mathbf{D}_2 = D_2\hat{\mathbf{x}}$ ($D_1 + D_2 = r_1 + r_2 + d$) connected by noninteracting springs attached to the beads at $\mathbf{R}_{1n}$ and $\mathbf{R}_{2n}$ and directed along $\Delta\mathbf{R}_n = \mathbf{R}_{2n} - \mathbf{R}_{1n}$ as illustrated in Fig. 3 *A*. The forces on the beads due to the *n*th spring are:

$$\mathbf{F}_{1n} = +F(|\Delta\mathbf{R}_n|)\Delta\mathbf{R}_n / |\Delta\mathbf{R}_n|, \tag{5}$$

$$\mathbf{F}_{2n} = -F(|\Delta\mathbf{R}_n|)\Delta\mathbf{R}_n / |\Delta\mathbf{R}_n|, \tag{6}$$

where $F(|\Delta\mathbf{R}_n|)$ is underlying force-extension relation for an individual spring, which is assumed to be given by Eq. 1. The total force is the sum over all springs:

$$\mathbf{F}_1 = \sum_{n=1}^{N} \mathbf{F}_{1n}, \tag{7}$$

$$\mathbf{F}_2 = \sum_{n=1}^{N} \mathbf{F}_{2n}. \tag{8}$$

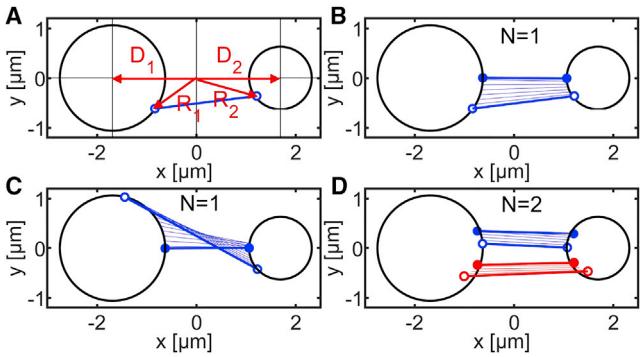

FIGURE 3 (*A*) Model setup for minimizing torque in a dual-trap multiple duplex DNA attachment simulation. (*B* and *C*) Typical torque minimizations for one ($N = 1$) attachment and (*D*) torque minimization for two ($N = 2$) attachments. The initial state is indicated by open circles and the final state by solid circles.

Each spring exerts torque on the beads. The torques on the beads due to the *n*th spring are

$$\mathbf{T}_{1n} = (\mathbf{R}_{1n} - \mathbf{D}_1) \times \mathbf{F}_{1n}, \tag{9}$$

$$\mathbf{T}_{2n} = (\mathbf{R}_{2n} - \mathbf{D}_2) \times \mathbf{F}_{2n}. \tag{10}$$

The total torque is the sum over all springs:

$$\mathbf{T}_1 = \sum_{n=1}^{N} \mathbf{T}_{1n}, \tag{11}$$

$$\mathbf{T}_2 = \sum_{n=1}^{N} \mathbf{T}_{2n}. \tag{12}$$

For a given configuration of *n* springs, the total force and total torque were calculated for each bead, the beads were rotated about an axis directed along $\mathbf{T}_1$ or $\mathbf{T}_2$ by a small angle $\theta = 1/100$ rad in a direction that reduces torque, and the calculation was repeated. Around 200 repeats were required to minimize torque, which was assumed to be the equilibrium configuration. At this equilibrium, the total force is directed along $\hat{\mathbf{x}}$ (to a good approximation). This calculation was then repeated for a range of bead separations, giving a (total) force *F* with separation *d*. An example of a minimization for $N = 1$ is shown in Fig. 3 *B*. The initial orientation of the spring is indicated by the thicker line terminated by open circles and the final orientation by the thicker line terminated by solid circles. Intermediate spring orientations are indicated with thinner lines. Here, the spheres turn so that the spring is oriented along $\hat{\mathbf{x}}$ where $d = d'$. A second example for $N = 1$, with a more extreme initial orientation, is shown in Fig. 3 *C* with the same result. Fig. 3 *D* shows the minimization for $N = 2$, with two springs, colored blue and red. The springs orient to a symmetric configuration. For more than two springs the final configuration is more complex and may lack symmetry.

As was suggested earlier, the final force-extension will depend on where the springs are attached to the beads. Here, we assume that attachments sites follow a biased Gaussian distribution, chosen here as a simple method of introducing normally distributed preferential attachment into the model, and compute initial attachment sites according to

$$\mathbf{R}_{1n} = r_1 \frac{(G_x + b)\hat{\mathbf{x}} + G_y\hat{\mathbf{y}} + G_z\hat{\mathbf{z}}}{\sqrt{(G_x + b)^2 + G_y^2 + G_z^2}} - D_1\hat{\mathbf{x}}, \tag{13}$$

$$\mathbf{R}_{2n} = r_1 \frac{(G_x - b)\hat{\mathbf{x}} + G_y\hat{\mathbf{y}} + G_z\hat{\mathbf{z}}}{\sqrt{(G_x + b)^2 + G_y^2 + G_z^2}} + D_2\hat{\mathbf{x}}, \tag{14}$$

where G_x, G_y, and G_z are random variables drawn (once, for each sphere and for each *n*) from a Gaussian distribution with a standard deviation $\sigma = 1$ with *b* being a dimensionless biasing parameter. Examples of biasing are shown in Fig. 4. When *b* is large, the attachments sites are quite localized on the beads. For smaller *b*, the attachment sites are spread more diffusely on the bead's surfaces.

Typical force-extensions, calculated using Eqs. 5, 6, 7, 8, 9, 10, 11, and 12, for the biased distributions Eqs. 13 and 14, are illustrated in Fig. 5. When the biasing is large, the resulting force-extension for separate *N* appears quite distinct. As biasing decreases, the force-extensions for separate *N* become less distinct and begin to overlap. An exception is $N = 1$, where the force-extension is insensitive to biasing; here, the spring orients to the *x* axis irrespective of the initial configuration.

To assess the utility of the multichain WLC approximation, simulated force-extension curves were fitted to Eq. 2. In the simulation, $l_p = 59.1$ nm and $l_c = 3.30\,\mu$m (based on (21)), $N = 1, 2, 3...7$ and $b = 2^{1.0}, 2^{1.2}, 2^{1.4}...2^{4.4}$ $(b = 2.00, 2.30, 2.64...21.1)$, and $r_1 = r_B = (2.12/2)$ μm and $r_2 = r_S = (1.26/2)$ μm were assumed. Two hundred force-extensions were simulated for each combination of *N* and *b*, so that 25.2k simulated force-extensions were fitted in total. Fitted statistics are reported in Fig. 6. Fig. 6 *A* gives examples of a poor fit and modestly good fit. The poorer fit still appears to capture the behavior of the simulation acceptably well. Included in the figure are the best-fit sum of the squares of the error (SSE), which is the parameter minimized, and a measure of the goodness-of-fit. Fig. 6 *B* gives the dependence of the average SSE on both *N* and *b*. The SSE shows a stronger dependence on *b*, increasing as *b* decreases, indicating that the approximation is poorer for smaller *b* values. The quality of the fit is less sensitive to *N*. Fig. 6 *C* shows the average fitted *N* with *b* and with model *N*. Fitted *N* and model *N* are in excellent agreement, except when both the *N* is large and *b* is small, where the fit is

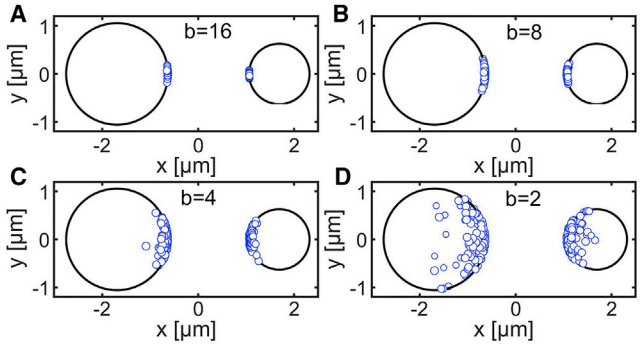

FIGURE 4 (*A–D*) Typical distributions of the attachment sites on the bead surface with the biasing parameter *b*.

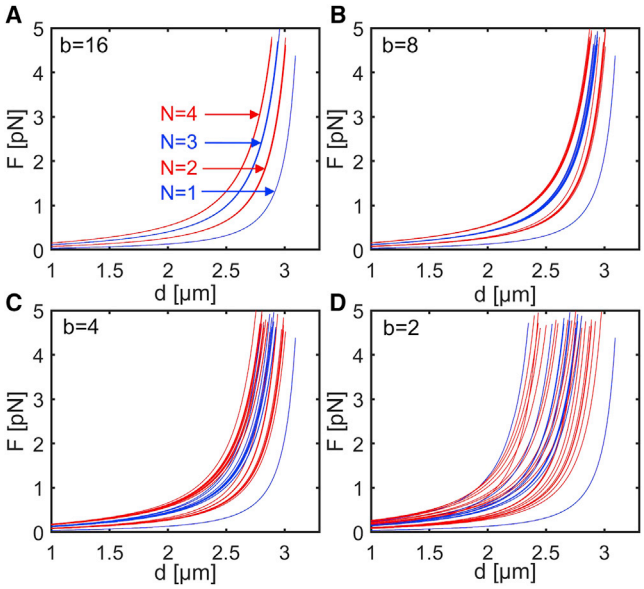

FIGURE 5 (*A–D*) Simulated force-extensions for $N = 1,\ 2,\ 3$, or 4 attachments with biasing parameter *b*.

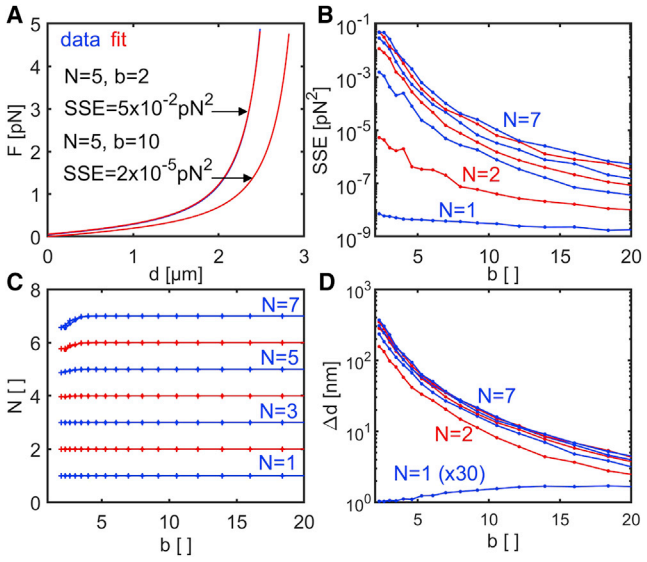

FIGURE 6 (*A*) Typical fits to simulated data using the two-parameter Eq. 2. Best-fitting sum of the squares of the error (SSE) is indicated. (*B*) Average fitted SSE with *b* and *N*. Average fitted (*C*) attachment number *N* and (*D*) excess extension Δd with biasing parameter *b*.

poorer. The agreement between the model and fit here indicate that the fit can be used to recover to *N*. Fig. 6 *D* gives the average fitted Δd with *b* and with model *N*. It would be expected that $\Delta d = 0$ when $N = 1$. For $N = 1$, Δd is very small, which confirms that the simulation and fit are reporting correctly. When $N \geq 2$, Δd increases with decreasing *b*. This seems sensible, as the attachment sites are scattered more widely on the spheres. The Δd dependence on *N* is weaker.

Experimental

To assess the model, we fitted experimental data. As noted above, both *d* and *F* include uncertainties Δr and ΔF. If these uncertainties are included, Eq. 2 becomes

$$F = N\frac{k_B T}{l_p}\left(\frac{1}{4}\left[\left(1-\frac{d+\Delta d+\Delta r}{l_c}\right)^{-2}\right] + \frac{d+\Delta d+\Delta r}{l_c} - \frac{1}{4}\right) + \Delta F. \tag{15}$$

This model has six independent parameters, characteristic chain lengths l_c and l_p, multiple duplex parameters *N* and Δd, and measurement uncertainties Δr and ΔF, and distinguishing between them could be expected to be difficult without constraints. Physically, it seems reasonable that the underlying l_c and l_p of the reference DNA will be the same across all measurements and that Δr will be common to all stretches with shared beads. Assuming that this is case, and that both single and multiple duplex stretches are observed for a given bead pair, fitting the data can be done in two steps: 1) the single duplex stretches are fitted to the conventional single duplex model to determine l_c, l_p, Δr, and ΔF (this step is split into two steps below); and 2) with l_c, l_p, and Δr fixed for a given bead pair, the multiple duplex stretches are fitted to the multiple duplex model to determine *N*, Δd, and ΔF. ΔF, which is associated with drift, was allowed to vary between fits. Specifically, the methodology followed was:

1. Fit all stretches to

$$F = \frac{k_B T}{l_p}\left(\frac{1}{4}\left[\left(1-\frac{d}{l_c}\right)^{-2}\right] + \frac{d}{l_c} - \frac{1}{4}\right) \tag{16}$$

to determine fit parameters l_c and l_p (two-parameter fit). $N = 1$ stretches are identified (discussed below) and median l_c and l_p are calculated from the $N = 1$ fits. For the $N = 1$ fits, the median fitted lengths were $l_p = 59.3$ nm and $l_c = 3.37$ μm.

2. Assuming median l_c and l_p values, fit $N = 1$ stretches to

$$F = N\frac{k_B T}{l_p}\left(\frac{1}{4}\left[\left(1-\frac{d+\Delta r}{l_c}\right)^{-2}\right] + \frac{d+\Delta r}{l_c} - \frac{1}{4}\right) + \Delta F \tag{17}$$

to determine fit parameters Δr and ΔF (two-parameter fit). The standard deviations of the fitted offsets were $\sigma_{\Delta r} = 23$ nm and $\sigma_{\Delta F} = 0.046$ pN.

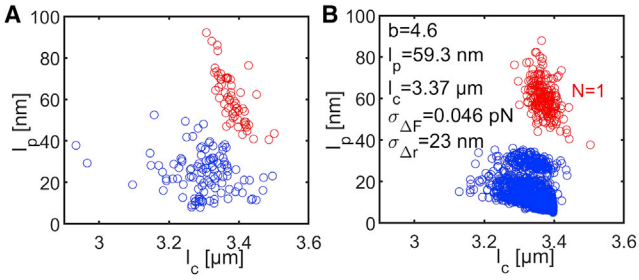

FIGURE 7 Fitted persistence length l_p and contour length l_c for fits to Eq. 16 for (*A*) experimental and (*B*) simulated data. Clustering observed here is used to identify $N = 1$ force-extensions.

3. Assuming median fitted l_c and l_p and Δr, fit the $N \geq 2$ stretches to Eq. 15; that is,

$$F = N\frac{k_B T}{l_p}\left(\frac{1}{4}\left[\left(1 - \frac{d + \Delta d + \Delta r}{l_c}\right)^{-2}\right] + \frac{d + \Delta d + \Delta r}{l_c} - \frac{1}{4}\right) + \Delta F,$$

to determine fit parameters *N* and Δd and ΔF (three-parameter fit).

Parameters, where not fixed, were fitted without constraints. Fitted l_p and l_c are shown in Fig. 7 *A*. The data appear to partition into an upper cluster at larger l_p and l_c values (*red*) and a lower cluster at smaller l_p and l_c values (*blue*). For investigation, force-extensions were simulated for $l_p = 59.3$ nm and $l_c = 3.37$ μm (from step 1), and for $b = 4.6$ (chosen for reasons discussed later), offsets Δr and ΔF, drawn randomly from Gaussian distributions with standard deviations $\sigma_{\Delta r} = 23$ nm and $\sigma_{\Delta F} = 0.046$ pN (from step 2) were added to the force and extension, and the resulting force-extensions were fitted as in step 1 above. Fitted l_p and l_c are shown in Fig. 7 *B*. Here the fitted data clearly partition into an upper cluster for which $N = 1$ and a lower cluster(s) for which $N \geq 2$. This clustering is similar to that seen in experimental data, justifying the partitioning assumed in step 1. It is further presupposed in step 1 that the fitted l_c and l_p do in fact average to the underlying (true) l_c and l_p value. This was tested and verified by fitting simulated data containing variable offsets Δr and ΔF, as discussed above.

The entire data set fitted is shown in Fig. 8 *A*, with the curves adjusted for fitted Δr and ΔF and colored according to the fitted *N*. $N = 1$ (*blue*) is on the extreme right and there is a gap between the $N = 1$ and $N \geq 2$ data, as expected. The $N \geq 2$ curves do overlap, suggesting that the associated biasing parameter *b* for the data is not especially large. Fig. 8 *B* shows a histogram of the fitted *N* values. The distribution indicates that smaller *N* values are more probable and shows

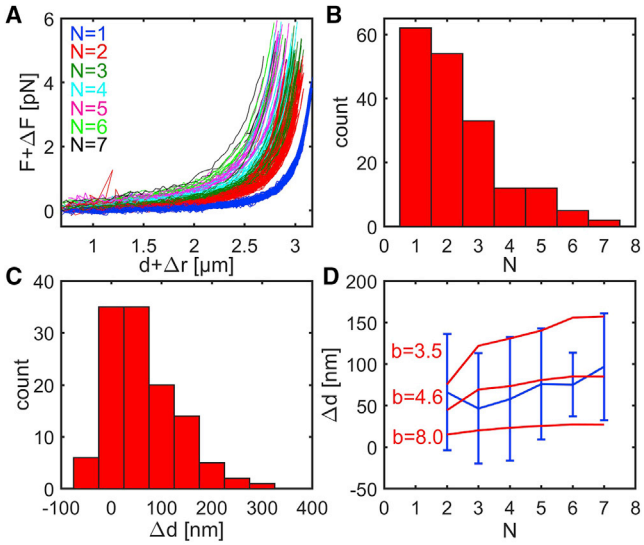

FIGURE 8 (*A*) Experimental force-extension including fitted offset corrections Δr and ΔF. Color indicates fitted *N*. Distribution of fitted (*B*) *N* and (*C*) Δd values. (*D*) Comparison of the experimental (*blue*) and simulated (*red*) fitted *N* and Δd (± 1 SD) for several values of *b*.

somewhat exponential behavior. We are cautious about attaching too much significance to the functional form of the histogram; only data in which both $N = 1$ and $N \geq 2$ were included in the analysis, and at large values of *N* the beads tend to get pulled out of the trap, ending the experiment with that pair of beads, which may skew the histogram to smaller *N*. Fig. 8 *C* shows a histogram of the fitted Δd values. This histogram is clearly skewed to positive Δd values. Physically, only positive Δd are expected, so the positive bias in this distribution helps support the model. Fig. 8 *D* shows the average (and standard deviation through the error bars) of Δd with respect to the *N* (*blue*). $\Delta d \approx 70$ nm over all measurements. The force-extension data were simulated for $l_p = 59.3$ nm and $l_c = 3.37$ μm, and for $N = 1, 2, 3 \ldots 7$ and $b = 2^{1.0}, 2^{1.2}, 2^{1.4} \ldots 2^{4.4}$ $(b = 2.00, 2.30, 2.64 \ldots 21.1)$ with 200 data sets computed for each combination of parameters and simulated data fitted to determine *N*, Δd, and ΔF. Average fitted Δd with respect to *N* is plotted for several *b* values in Fig. 8 *D* (*red*). The comparison between the fits to the experimental and simulated data indicated that $b \approx 5$, suggesting that attachment sites are moderately biased and somewhat favor attachment at sites closer to the longitudinal axis.

DISCUSSION

In this work, we assume that we can represent multiple chains in a dual optical trap stretch experiment as noninteracting nonlinear springs, attached according to a biased distribution over the surface of the two

beads. Force extension was computed by minimizing torque for a given configuration, and it was demonstrated that the resulting force-extension could be parameterized by modifying the conventional WLC model to include the number of chains *N* and a characteristic length Δd, which can be determined by fitting this calculated force-extension. The model was tested by fitting experimental force-extension data for reference DNA to the multichain WLC model. It was found that: 1) unconstrained fits to the data were good; 2) the fitted Δd was overwhelmingly positive (as is required physically); 3) the probability of obtaining *N* tethers decreases monotonically with increasing *N* (as seen in Fig. 8 *B*), which seems physically plausible (although the mechanism is unclear); 4) the distributions of fitted *N* and Δd across the data varied fairly smoothly (as seen in Fig. 8, *B* and *C*); and 5) that the variation of *N* and Δd were broadly consistent with that predicted by the torque minimization model for particular biasing (as seen in Fig. 8 *D*). We consider this good evidence that we have successfully tested the model described.

In the analysis conducted here, each experimental or simulated stretch was fitted separately. A global fitting method could be implemented programmatically to fit the data. To globally fit the data, we would anticipate assuming (as before) that l_c and l_p were constant across all measurements, Δd was constant across shared beads, and that *N*, Δd, and ΔF varied between stretches. There is a subtle issue with this approach, however. While l_c, l_p, Δr, Δd, and ΔF vary continuously, *N* varies discretely. This discrete variation creates issues for minimization methods in which it is assumed that parameter space varies continuously. *N* was fitted in all cases here by separately fitting the other parameters for given $N = 1, 2 \ldots 10$ and choosing the *N* that minimized the overall SSE. This method, which is partly a conventional fit and partly a parameter search, does not scale easily to multiple data sets.

Many DNA stretching experiments seek to determine l_p and l_c. In the results section, we fitted experimental data to l_p and l_c to identify $N = 1$ single duplex stretches. Once these stretches are identified, and if an estimate of Δr is not required (or if Δr can be neglected), l_p and l_c can be more accurately estimated by fitting stretches to l_p and l_c and ΔF. This is illustrated in Fig. 9. Here we calculate force-extension according to the WLC model including the uncertainties Δr and ΔF:

$$F = \frac{k_B T}{l_p}\left(\frac{1}{4}\left[\left(1 - \frac{d + \Delta r}{l_c}\right)^{-2}\right] + \frac{d + \Delta r}{l_c} - \frac{1}{4}\right) + \Delta F \tag{18}$$

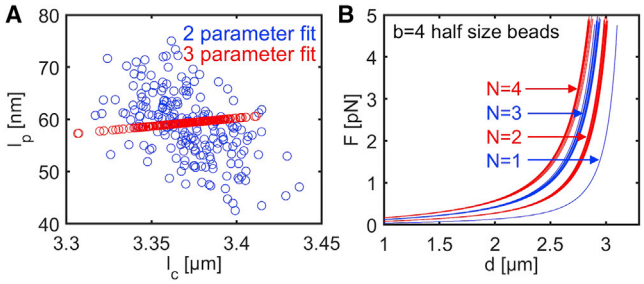

FIGURE 9 (*A*) Fitted parameter l_p and l_c to a two-parameter (l_p and l_c, *blue*) or three-parameter (l_p, l_c, and ΔF, *red*) model when simulated data contains random offsets ΔF and Δr. (*B*) Narrowing of the distribution of simulated force-extension produced by reducing bead size by half (compare with Fig. 4 *C*).

for $l_p = 59.3$ nm and $l_c = 3.37$ μm, and with Δr and ΔF drawn randomly from Gaussian distributions with standard deviations $\sigma_{\Delta r} = 16.9$ nm and $\sigma_{\Delta F} = 0.05$ pN (so that $\sigma_{\Delta r}/(r_1 + r_2) = \sigma_{\Delta F}/F_{max} = 1\%$), and fit the data to Eq. 18 to determine l_p and l_c (assuming $\Delta r = \Delta F = 0$) or l_p, l_c, and ΔF (assuming $\Delta r = 0$). Fitted l_p and l_c for the two- and three-parameter fits are shown in Fig. 9 *A*. Clearly the three-parameter fit reduces variation in the fitted l_p, and we have used this three-parameter model to estimate l_p and l_c in previous experimental work. Results are similar if data are fitted to l_p, l_c, and Δr (assuming $\Delta F = 0$). While it is possible to fit analytic data to all four parameters, this is not practical for experimental data, owing to noise (which is non-Gaussian in this sort of experiment (28)).

As in magnetic tweezers trapping, torque can be applied to the optically trapped beads by manipulating the spin or orbital angular momentum of the photons that produce the optical trap (29). This torque can be included in the earlier calculations and may be useful for probing number and distribution of attachments. The effects of this torque on calculated stretching behavior are briefly illustrated in the supporting material.

Reducing the bead size could be expected to help identify the number of duplexes present. This is illustrated in Fig. 9 *B* where the force-extension curves are calculated as in Fig. 4 with beads half the diameter of that assumed earlier ($r_1 = r_B = (2.12/4)$ μm and $r_1 = r_S = (1.26/4)$ μm) and with $b = 4$. Comparing Fig. 9 *B* with Fig. 5 *C* it can be seen that the force-extensions for the smaller beads show less overlap, making it easier to distinguish between the sets of curves. This improvement due to the reduction in bead size presupposes that the biasing parameter *b* does not depend on size; this would need to be verified experimentally.

For attachment to occur, the handles must make contact with the treated surfaces. Reducing the probability of contact will reduce the number of attachments

observed. Strategies that can be expected to reduce this probability include decreasing the concentration of DNA on the beads, increasing minimum spacing between surfaces during the experiment, and decreasing the dwell time at the minimum spacing. Reducing attachment probability will increase the time required for an attachment to occur and increase the overall measurement duration. This can be problematic in laser tweezers experiments in which continuous infrared irradiation can significantly reduce binding probabilities (30). Ultimately, because attachment between the handles and surfaces is fundamentally stochastic, multiple attachments can be expected if the number of measurements is sufficient. The work described here helps understand the effects of these multiple attachments on force-extension measurements and how such data might be excluded from analysis, if required.

CONCLUSION

Multiple duplex DNA attachments in a dual-trap force-extension experiment were modeled by minimizing the torque produced by noninteracting nonlinear springs attached at random locations on the bead surfaces. Guided by simulation, and with an awareness of common sources of error, which include offsets in the force ΔF and bead separation Δr (due to uncertainties in bead radii), a large set of experimental data were fitted to a multichain WLC model to determine persistence l_p and contour l_c lengths, number of attachments *N*, and an average excess extension Δd. Based on the measured dependence of Δd on l_p and l_c, the random attachment sites appear to be moderately biased toward the nearer surfaces of the beads. The multichain WLC model, including sources of error, depends on the six parameters l_p, l_c, *N*, Δd, ΔF, and Δr, and it is not reasonable to expect to separate these parameters in a fit without systematic constraints, as was done here. In a more unconstrained case the multichain WLC is best used as a guide to what might be expected if multiple attachments were present and how to mitigate these effects in a dual-trap force-extension experiment.

SUPPORTING MATERIAL

Supporting material can be found online at https://doi.org/10.1016/j.bpr.2022.100045.

AUTHOR CONTRIBUTIONS

A.R., with feedback from M.A.K.W. and G.B.J., designed and performed the research and wrote most of the manuscript.

DECLARATION OF INTERESTS

The authors declare no competing interests.

ACKNOWLEDGMENTS

The authors thank Lisa M. Kent for synthesizing the DNA used. This work was supported by the Royal Society of New Zealand Marsden Fund (grant number MAU1810).

REFERENCES

1. Gross, P., N. Laurens, …, G. J. Wuite. 2011. Quantifying how DNA stretches, melts and changes twist under tension. *Nat. Phys.* 7:731–736.
2. Bustamante, C., S. B. Smith, …, D. Smith. 2000. Single-molecule studies of DNA mechanics. *Curr. Opin. Struct. Biol.* 10:279–285.
3. Marko, J. F., and E. D. Siggia. 1995. Stretching DNA. *Macromolecules.* 28:8759–8770.
4. Salomo, M., K. Kegler, …, F. Kremer. 2006. The elastic properties of single double-stranded DNA chains of different lengths as measured with optical tweezers. *Colloid Polym. Sci.* 284:1325–1331.
5. Wang, M. D., H. Yin, …, S. M. Block. 1997. Stretching DNA with optical tweezers. *Biophys. J.* 72:1335.
6. Fuller, D. N., G. J. Gemmen, …, D. E. Smith. 2006. A general method for manipulating DNA sequences from any organism with optical tweezers. *Nucleic Acids Res.* 34:e15.
7. Biancaniello, P. L., A. J. Kim, and J. C. Crocker. 2008. Long-time stretched exponential kinetics in single DNA duplex dissociation. *Biophys. J.* 94:891–896.
8. Yogo, K., T. Ogawa, …, K. Kinosita, Jr. 2012. Direct observation of strand passage by DNA-topoisomerase and its limited processivity. *PLoS One.* 7:e34920.
9. van der Horst, A., and N. R. Forde. 2008. Calibration of dynamic holographic optical tweezers for force measurements on biomaterials. *Opt. Express.* 16:20987–21003.
10. Wallin, A. E., H. Ojala, …, E. Haeggström. 2009. High-resolution optical tweezers for investigating DNA-binding/translocating molecular motors. *In* Optical Trapping and Optical Micromanipulation VI. International Society for Optics and Photonics, p. 740007.
11. Wasserman, M. R., and S. Liu. 2019. A tour de Force on the double helix: exploiting DNA mechanics to study DNA-based molecular machines. *Biochemistry.* 58:4667–4676.
12. King, G. A., E. J. Peterman, and G. J. Wuite. 2016. Unravelling the structural plasticity of stretched DNA under torsional constraint. *Nat. Commun.* 7:1–7.
13. Ott, W., M. A. Jobst, …, M. A. Nash. 2017. Single-molecule force spectroscopy on polyproteins and receptor-ligand complexes: the current toolbox. *J. Struct. Biol.* 197:3–12.
14. Javadi, Y., J. M. Fernandez, and R. Perez-Jimenez. 2013. Protein folding under mechanical forces: a physiological view. *Physiology.* 28:9–17.
15. Lipfert, J., G. M. Skinner, …, N. H. Dekker. 2014. Double-stranded RNA under force and torque: similarities to and striking differences from double-stranded DNA. *Proc. Natl. Acad. Sci. U S A.* 111:15408–15413.
16. Rickgauer, J. P., D. N. Fuller, and D. E. Smith. 2006. DNA as a metrology standard for length and force measurements with optical tweezers. *Biophys. J.* 91:4253–4257.
17. delToro, D., and D. E. Smith. 2014. Accurate measurement of force and displacement with optical tweezers using DNA molecules as metrology standards. *Appl. Phys. Lett.* 104:143701.

18. Bustamante, C., J. F. Marko, …, S. Smith. 1994. Entropic elasticity of lambda-phage DNA. *Science.* 265:1599–1600.

19. Bouchiat, C., M. D. Wang, …, V. Croquette. 1999. Estimating the persistence length of a worm-like chain molecule from force-extension measurements. *Biophys. J.* 76:409–413.

20. Farré, A., A. van der Horst, …, N. R. Forde. 2010. Stretching single DNA molecules to demonstrate high-force capabilities of holographic optical tweezers. *J. Biophotonics.* 3:224–233.

21. Suei, S., A. Raudsepp, …, M. A. Williams. 2015. DNA visualization in single molecule studies carried out with optical tweezers: covalent versus non-covalent attachment of fluorophores. *Biochem. Biophys. Res. Commun.* 466:226–231.

22. Raudsepp, A., L. M. Kent, …, M. A. Williams. 2018. Overstretching partially alkyne functionalized dsDNA using near infrared optical tweezers. *Biochem. Biophys. Res. Commun.* 496:975–980.

23. Bustamante, C. J., Y. R. Chemla, …, M. D. Wang. 2021. Optical tweezers in single-molecule biophysics. *Nat. Rev. Methods Primers.* 1:1–29.

24. Strick, T., J.-F. Allemand, …, V. Croquette. 1998. Behavior of supercoiled DNA. *Biophys. J.* 74:2016–2028.

25. Charvin, G., A. Vologodskii, …, V. Croquette. 2005. Braiding DNA: experiments, simulations, and models. *Biophys. J.* 88:4124–4136.

26. Neuman, K. C., G. Charvin, …, V. Croquette. 2009. Mechanisms of chiral discrimination by topoisomerase IV. *Proc. Natl. Acad. Sci. U S A.* 106:6986–6991.

27. Johnson, K., and W. Thomas. 2018. How do we know when single-molecule force spectroscopy really tests single bonds? *Biophys. J.* 114:2032–2039.

28. Burnham, D. R., I. De Vlaminck, …, C. Dekker. 2014. Skewed Brownian fluctuations in single-molecule magnetic tweezers. *PLoS One.* 9:e108271.

29. Jones, P. H., O. M. Marago, and G. Volpe. 2015. Optical Tweezers: Principles and Applications. Cambridge University Press.

30. McCauley, M. J., L. Furman, …, M. C. Williams. 2018. Quantifying the stability of oxidatively damaged DNA by single-molecule DNA stretching. *Nucleic Acids Res.* 46:4033–4043.